Journal of Marine Research, 68, 237–257, 2010

Patchiness in internal tidal beams

by Hans van Haren[1,2], Leo R. M. Maas[1] and Theo Gerkema[1]

ABSTRACT

Results are presented from measurements on internal tides and near-inertial motions, obtained using deep-towed acoustic Doppler current profilers along a single transect over the continental slope in the Bay of Biscay and, in another experiment, over a flank of Great Meteor Seamount in the Canary Basin. Each measurement lasted two days and involved repeated passage of the same track, making it possible to extract by harmonic analysis the semidiurnal (and, over Great Meteor Seamount, also the combined diurnal/near-inertial) signal. In the Bay of Biscay, the transect covered by the towing was sufficiently long to follow the internal semidiurnal tidal beam for large-scale stratification well beyond its detachment from the continental slope. Here, "large-scale" stratification is computed from CTD-observations over vertical scales O(100 m). Remarkably, the beam is much more distinct in its phase field, which is coherent throughout, than in its amplitude, which shows a lot of patchiness and small-scale near-horizontal layering. The hypothesis is put forward that this may be associated with the interaction between internal waves and variations in space and time of stratification. In part, it may be attributable to aliased, weaker, near-inertial beams that are more horizontal for large-scale stratification. The diurnal/inertial and, to a lesser extent, semidiurnal signals over Great Meteor Seamount show the same phenomenon, but here co-phase and co-amplitude bands are more distinctly nearly horizontal, indicative of near-horizontal energy propagation at all frequencies investigated.

1. Introduction

In recent decades, abundant evidence has been gathered of intermittent behavior in internal wave signals, especially internal tides; they "come and go" (Wunsch, 1975). The classic reference is Magaard and McKee (1973). They demonstrated the occurrence of intermittency in Eulerian current meter records from a site in the western North Atlantic. Their band-pass filtered records showed a semidiurnal signal whose envelope was highly irregular, both in its time-scale and its amplitude. Intermittency of this kind has been attributed to variability in the internal wave "background" field, viz. to variability in the stratification near the shelf break, an important source of internal tides (Huthnance and Baines, 1982; Baines, 1986), or to irregularities in the (internal tide creating) cross-slope currents, due to wind and upwelling (Sandstrom, 1991). In either case, the background field is subject to irregular subinertial perturbations, which affect both the generation and

1. Royal Netherlands Institute for Sea Research (NIOZ), P. O. Box 59, 1790 AB Den Burg, The Netherlands.
2. Corresponding author. ***email: hans.van.haren@nioz.nl***

propagation of internal waves. Or, at a given position away from a source, phase and amplitude of an internal wave will change due to background variations at the source and along the wave's path.

Previous observations showing intermittency (some of them mentioned above) involved time-series at fixed positions, essentially point measurements. A complementary perspective is to examine the spatial structure and coherence (or lack thereof) of the internal-wave field. Such observations, providing a spatially synoptic view of an internal wave pattern, are essential for answering the question of how the intermittency in time translates into the spatial pattern. Indeed, the question is whether spatially coherent internal wave "beams" may be found at all. Earlier measurements on internal tidal beams were inconclusive on this point, because they were based either on moored observations separated by at least a couple of kilometers horizontally (deWitt *et al.,* 1986) or on even more widely separated sites of CTD yoyo-ing (Pingree and New, 1991). More in general, open ocean observations show an internal wave field that becomes incoherent over short O(km) horizontal spatial scales (Briscoe, 1975; Saunders, 1983; van Haren, 2004).

Few spatially synoptic observations have been reported in the literature. Lueck and Mudge (1997) and Lien and Gregg (2001) presented spatial distributions of the turbulent dissipation rate over a coastal ridge, based on repeated microstructure profiler data; this gives, albeit indirectly, an indication of the spatial distribution of the internal tide near a potential source. They found that the scattered, non-smooth distribution of enhanced dissipation followed the direction of the theoretically predicted (downward) internal tidal beam reasonably well. Martin *et al.* (2006) sailed multiple transects using undulating CTD and shipborne acoustic Doppler current profiler (ADCP) to map internal wave energy emanating from the Hawaiian Ridge in the upper 300 m near the surface.

More direct were observations made with a towed ADCP over the shelf edge in the Bay of Biscay (Lam *et al.,* 2004; Gerkema *et al.,* 2004). By covering the same transect ten times within one day, it was possible to distil the semidiurnal internal tide from the data by making harmonic fits, which were then decomposed into the spatial distributions of amplitude and phase. The presence of an internal tidal beam was particularly clearly seen in the latter, with phases propagating upward, consistent with downward energy propagation. The spatial distribution of the amplitude seemed overall to be coherent, too. However, these measurements involved only short transects of about 14 km horizontally down to about 700 m and were not sufficient to see the beam becoming detached from the slope.

Here we extend previous findings by presenting results of new towed-ADCP measurements over longer and deeper tracks along a single cross-slope transect. We carried out such measurements at two locations, down to 1400 m. The first one was in the Bay of Biscay (BB), in April 2005; here we covered a cross-slope transect of about 37 km, over the continental slope (Fig. 1). The second was over Great Meteor Seamount (GMS), a guyot in the Canary Basin, in May 2006; here the transect was about 22.5 km long (Fig. 2). Internal tides are known to feature in both regions. In BB, they have been widely studied (e.g., Pingree and New, 1991), and are known to be strong, with semidiurnal internal tidal

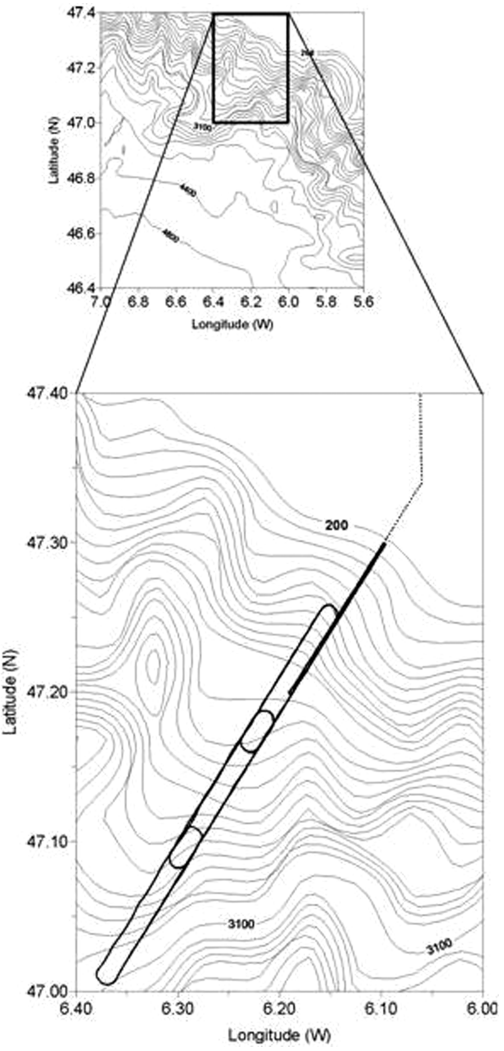

Figure 1. Part of the continental slope in the Bay of Biscay "BB" off Brittany (F), with the towed-ADCP "DTV" tracks superposed in the detail. Depth in m. The wide tracks are "deep," when DTV is at 800 m, the narrow track "shallow," when the DTV is at 200 m. Along-slope x-axis is positive to the North-west, y-axis is positive off-slope.

energy fluxes as large as 10 kW m^{-1} (Gerkema *et al.,* 2004). Over GMS, such energy fluxes are about four times smaller (Gerkema and van Haren, 2007); integrated along the circumference of the plateau of the seamount, this amounts to a total conversion from barotropic to baroclinic semidiurnal tidal energy of about 0.3 GW. (To put this into perspective: this is sixty times smaller than the value found for the Hawaiian Ridge, viz.

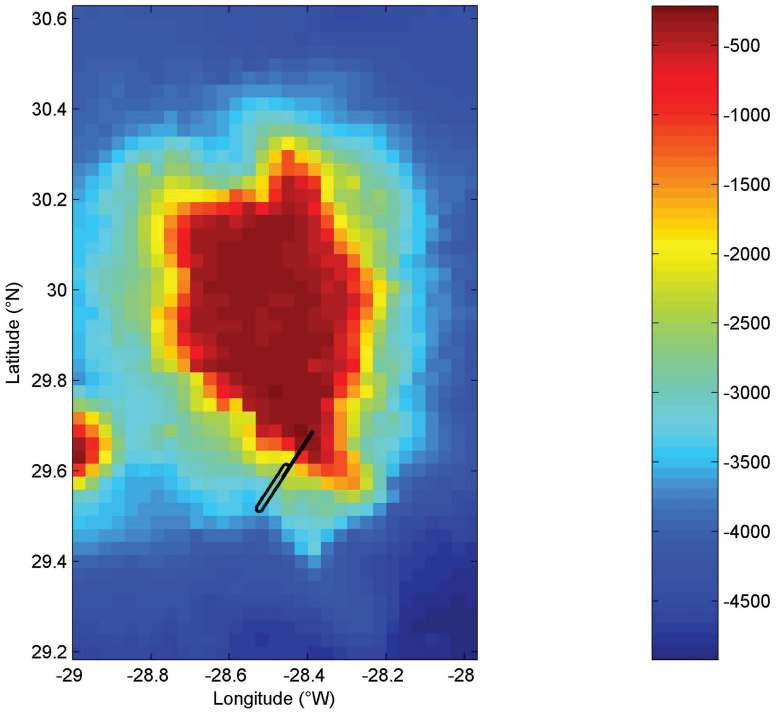

Figure 2. Great Meteor Seamount topography in the Canary Basin, with DTV-tracks consisting of a single shallow and a single deep portion. Colors indicate depth in m. Axes-direction as in Figure 1.

18 GW for semidiurnal lunar M_2 (Klymak *et al.,* 2006); but, then, the Hawaiian Ridge consists of some 80 seamounts, so *per seamount* the conversion is rather similar!)

The main purpose of the present measurements, and of the present paper, is to examine the spatial coherence of the internal tidal beams at the two locations. The paper is organized as follows. In Section 2, we describe the technical aspects of the instruments. In Section 3, we present the analysis of the measurements made in the Bay of Biscay; and, in Section 4, those made over Great Meteor Seamount. In Section 5, we state some general conclusions that these observations allow us to draw.

2. Instruments, observational set-up and data analysis

The measurements were made using a deep-towed vehicle (DTV), consisting of an aluminum frame with 8 Benthos glass sphere floats each supplying 25 kg buoyancy, lead balance weights, and two 75 kHz Teledyne RDI-Longranger ADCPs, one looking upward, the other downward (Fig. 3). Both ADCPs were programmed to cover 600 m vertical range in 10 m vertical bin-intervals. They sampled the backscatter of 7 acoustic pings every 20 s using a transmission length of 9.85 m, only storing 20-s ensemble averages. The sampling

Figure 3. DTV with up- and down-looking ADCP's pulled sideways above deck.

ensures instrumental error for horizontal currents to be within 2.5×10^{-2} m s^{-1} per stored ensemble. The instruments pinged asynchronously to avoid cross-talk. The near-neutrally buoyant vehicle was attached via a 50-m nylon line to a 1350 kg weight and an additional

1200 kg weight holding a SeaBird pressure sensor. The entire package was towed using a Kevlar line and electric cable. The ADCPs stored data internally, but pressure information was also available on-line (however, due to a problem with the cable, the on-line connection did not function during the observations over Great Meteor Seamount).

The measurements with the DTV were performed at a speed of 3 ± 0.3 knots. This margin of variation in the ship's speed corresponds with a variation in depth of the DTV of ±20 m as was found after extensive tests (van Sebille *et al.,* 2004). Varying background currents similarly contribute to variations in the DTV's depth. As pressure was recorded, we were able to correct for these variations afterwards. When on-line pressure was available, we could minimize depth variations by slightly adjusting the ship's speed but post-processing corrections were always needed. Moreover, the current velocities measured by the ADCPs needed to be corrected for the ship's own speed; this was done by subtracting the average current speed and direction of all bins in the entire local vertical range, excepting erroneous ("NaN") data. This also removed a substantial part of the barotropic tide. (Using the ship's GPS-data proved impossible as the DTV was towed on a loosely tethered cable.)

The DTV was towed either at approximately 200 m depth with a fixed length of 220 m cable paid out (in the shallowest part) or at approximately 800 m depth with a fixed length of 1350 m paid out (in the deeper parts). In the latter case, the ADCPs together covered a vertical range from 200 m beneath the surface down to about 1400 m (since the range of each ADCP is about 600 m), implying that there are no data for the upper 200 m over the deeper parts. This is not a serious lacuna, for the main beam is expected to be the downward going one, descending to greater depths as it propagates away from the slope.

For the Bay of Biscay a transect of 37 km was subdivided into four tracks, the two shallowest of which were chosen to have a considerable overlap (Fig. 1). This was done in view of the steep slope, which makes it necessary to cover great water depths even at short distances from the shelf edge. In Figure 4b, the first track runs from 0 to 13 km, the second from 7 to 18 km, the third from 17 to 28 km, and the fourth from 27 to 37 km. In the first track, the towing depth was 200 m; in the other three, 800 m. The horizontal white bands at 200 m and 800 m, respectively, are due to the fact that there are no data near the depth at which the DTV is towed. The vertical white bars indicate the different sections and mask processing problems at the turning points where data are close together in time. All tracks were sailed five times in about 12.5 hours (i.e. each position visited five times).

Over Great Meteor Seamount, a similar procedure was followed, but here the transect of 22.5 km was divided into two tracks (Figs. 2, 4d). Along the shallowest track, the DTV was towed at 200 m over a length of 12.5 km; along the deeper track, at 800 m over a length of 11 km. The tracks were taken such that they had an overlap of about 1 km (hence the total length of 22.5 km). First, the shallow track was traversed 11 times (i.e. each position on the track was visited 11 times in total, with six off-slope sailings and five return sailings), during a time span of about 26 hours. Then the deep track was equally traversed 11 times, during a time span of 27 hours.

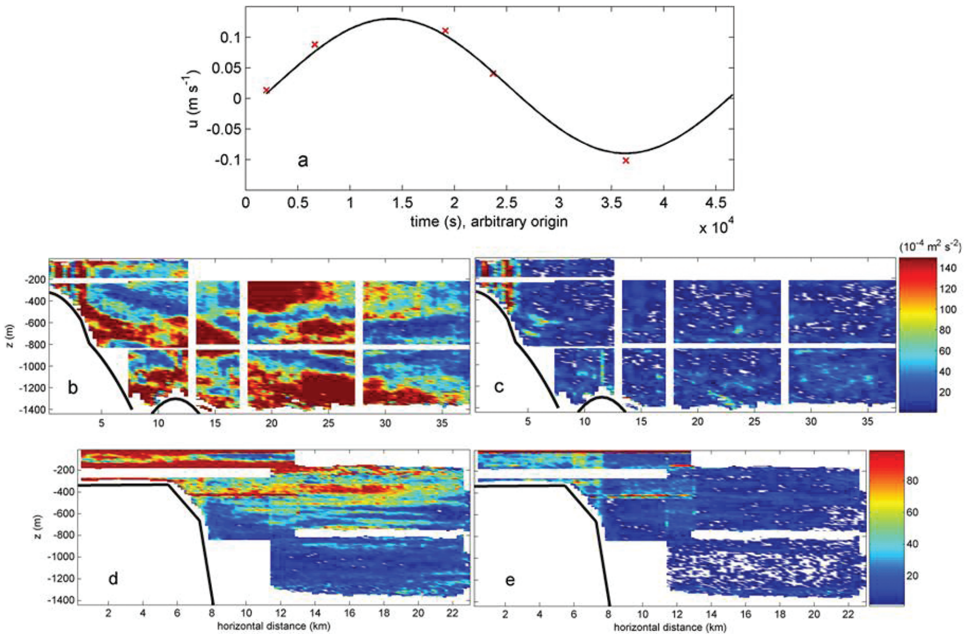

Figure 4. (a) Large-amplitude five-point data time series and its tidal harmonic fit, from BB. (b) Total variance of harmonic motions in cross-slope BB (colour scale as in (c)). (c) Rest-variance after subtraction of explained semidiurnal harmonic in cross-slope BB. (d) As (b), but for GMS (color scale as in (e)). (e) Rest-variance after subtraction of explained diurnal and semidiurnal harmonics in cross-slope GMS. Note the different colour-scale compared to BB.

Strictly speaking, the off-slope and return tracks were different in that the latter was shifted in the transverse (i.e. along-slope) direction (especially so with the deeper tracks, see Figs. 1, 2); this was necessary in order to ensure that the ship could retain its constant speed with the DTV at the required depth along a track. In the analysis, however, we treat the off-slope and return tracks as if they were identical.

So, for all tracks, each position is covered by five datapoints within one semidiurnal tidal period. This is marginally enough to make a fit, per horizontal Cartesian current component, along- and cross-slope, with a harmonic sinusoid of that period (see the example in Fig. 4a). However, the coarse sampling results in an aliasing of all higher harmonics, such as M_4 since the Nyquist period is five to six hours. Furthermore, the sampling does of course not resolve individual semidiurnal tidal constituents such as M_2 and S_2. In the Bay of Biscay also the inertial frequency is not resolved, although inertial energy is rather weak, $<10\%$ variance of M_2 (van Haren *et al.,* 2002). In the case of Great Meteor Seamount, where tracks are covered during more than a day, the diurnal period is being resolved besides the semidiurnal, but here we cannot distinguish individual diurnal tidal components (such as O_1 or K_1) or the inertial period, which at this latitude (30°N) is diurnal, too.

Before making a harmonic fit, the data were smoothed horizontally by taking the average over intervals of 250 m along a track (corresponding to about eight ensemble-samples in time). Per constituent, phase is determined with respect to a fixed common date and time. For the Bay of Biscay, at each position a fit was made for each horizontal current component involving two constituents: a constant (i.e. time-mean) one and a semidiurnal sinusoid. For Great Meteor Seamount, a diurnal sinusoid was included as well. In order to estimate how large a part of the signal is thus explained, we calculated the rest-variance by subtracting the signals of tidal and time-mean constituents from the original signal, and taking the mean of squared differences. The typical order of magnitude of the rest-variance is 10^{-4} m^2 s^{-2} (Fig. 4c, e). Relatively, this "error" amounts to 20 $\pm$ 10% of the explained harmonic variance, but in areas where amplitudes are small, it may be as large as 100%. The upshot is that wherever considerable internal tidal energy is present, the harmonic fit explains more than 70% of the original signal; we are thus confident that the fit provides a sufficiently solid basis for further analysis.

3. Bay of Biscay

In the Bay of Biscay, the direction of all tracks was 212°TN (return: 32°TN), with the shallowest track starting at 47°17.689′N, 06°05.956′W, where water depth is 241 m (Fig. 1). At the end of the total transect (47°00.188′N, 06°21.908′W), water depth is 3145 m. Over the entire period (23–25 April 2005) weather conditions were reasonably good and towing was possible throughout, even during a wind-spell with speeds between 14 and 17 m s^{-1} (7 Beaufort). Springtide was at 25 April.

Both for the along-slope velocity component u and the across-slope v, the harmonic analysis yields a constant time-mean amplitude as well as semidiurnal tidal signal estimates of phase and amplitude in two-dimensional views in a plane spanned by the cross-slope direction and the vertical. The results are gathered in Figures 5 and 6. Henceforth, we present current amplitude, the direct harmonic result, rather than its variance as an indicator for kinetic energy variations and propagation directions. The four tracks combined give a reasonably coherent picture, with generally smooth transitions between the different tracks.

We consider first the phase (Fig. 5). The most conspicuous feature is the diagonally oriented co-phase bands, from the slope downward into the deep ocean. They are parallel to the solid lines drawn in the figures. These lines are not merely auxiliary in emphasizing the structure, but they actually represent the direction of energy propagation along characteristics $\mu_{\pm}$ according to the general expression from internal-wave theory for large-scale "mean" buoyancy frequency N computed from local CTD-observations over, say, vertical scale $\Delta z = 100$ m (LeBlond and Mysak, 1978; Gerkema and Shrira, 2005),

$$\mu_{\pm} = \frac{f f_s \pm (f^2 f_s^2 + (\sigma^2 - f^2)(N^2 - \sigma^2 + f_s^2))^{1/2}}{N^2 - \sigma^2 + f_s^2} = -\cot\theta, \qquad (1)$$

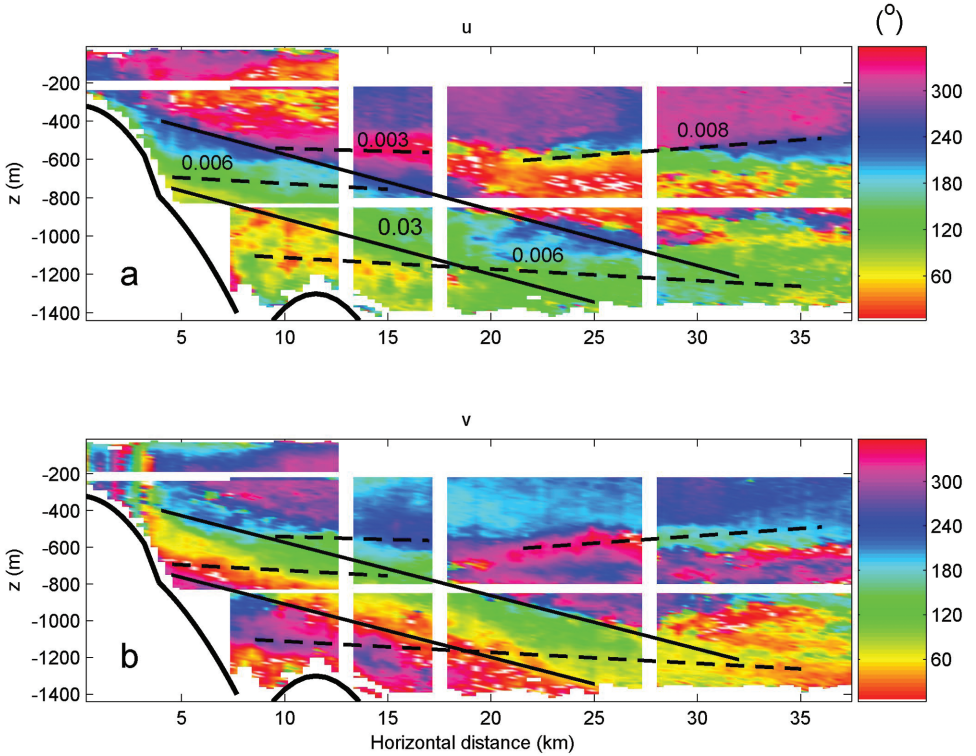

Figure 5. Semidiurnal tidal phase of (a) along-slope and (b) cross-slope component observed in BB. The white horizontal lines indicate the transitions between up- and downlooking ADCP's, the vertical ones designate the four different tracks. Note the relatively large overlap between the "shallow" track to the left and the first "deep" track. Theoretical slopes (solid, dashed black lines) are computed for particular σ, N using either semidiurnal or near-inertial internal wave frequencies (cf, Table 1, Fig. 7a). They can be placed anywhere in the domain, considering N. They can be used for reference of particular pattern-directions but it is noted that they can match any one or more of four panels in Figures 5a,b and 6a,b. Here, solid lines indicate approximate slopes for semidiurnal tide in large-scale (Δz = 100 m) stratification or near-inertial motions in weak stratification (slopes of 0.030, e.g., for $\sigma = M_2$, N = 27f and σ = 1.00f, N = 8f, cf Table 1). Sample dashed lines may represent slopes for near-inertial motions in strong stratification or semidiurnal motions in extremely strong, thin-layer stratification (slope 0.003 (e.g., σ = 1.01f, N = 45f and σ = 1.00f, N = 27f), 0.006 (σ = 1.01f, N = 30f) and 0.008 ($\sigma = M_2$, N = 100f and σ = 0.9999f, N = 15f)).

where θ is the angle between the vertical and the direction of energy propagation, σ the frequency, semidiurnal in this case, $f = 2\Omega \sin \varphi$ the Coriolis parameter at latitude φ, Ω the earth rotational vector, and $f_s = f_h \sin \alpha$, α the wave angle with respect to the East, including the horizontal component $f_h = 2\Omega \cos \varphi$. The latter has only importance in very weak stratification and for the propagation of near-inertial motions, including just sub-inertial ones.

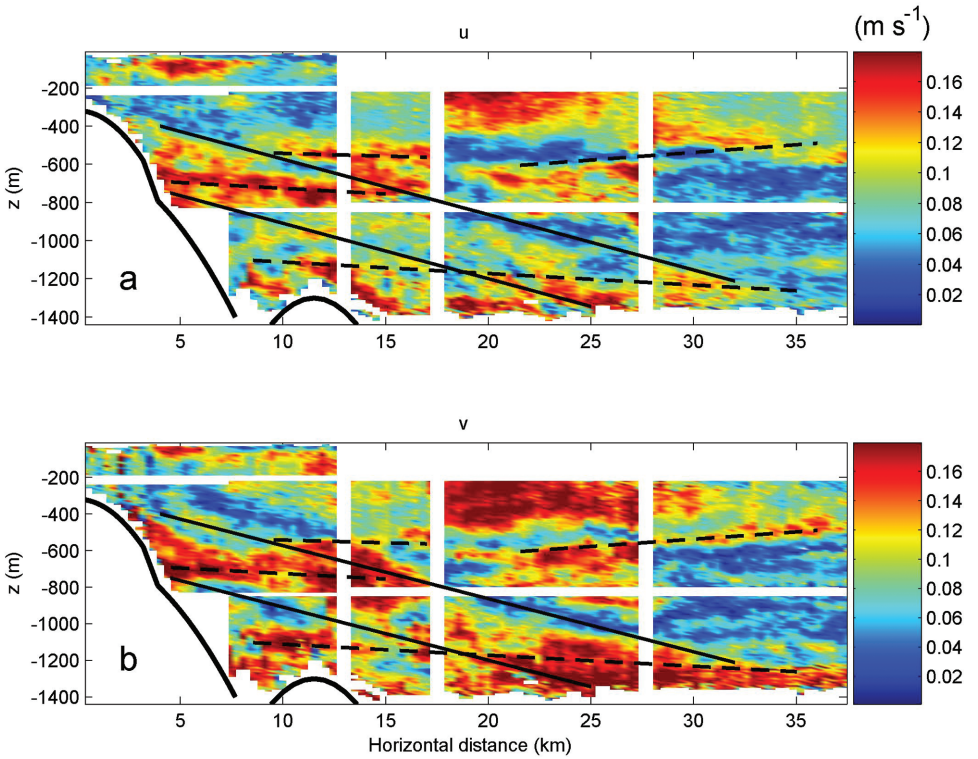

Figure 6. As Figure 5 but for the amplitude. The straight dashed and solid lines are identical to those in Figure 5.

According to the theory, energy propagation must be perpendicular to phase propagation, or, in other words, parallel to co-phase lines. For example, for internal inertio-gravity waves in the traditional but limited range $f < \sigma < N$, $N > f$ estimated over any vertical scale, the two are vertically opposed, i.e. if phases propagate vertically upward, energy propagates vertically downward. In near-homogeneous layers $N < f$, they have the same sign for propagating sub-inertial waves. Propagation directions are ambiguous for trapped motions (Gerkema and Shrira, 2005; van Haren, 2006).

Now, from Figure 5 we see that phases paralleling the solid lines here propagate upward, which is consistent with energy propagation from the slope down into the deep ocean considering the large-scale stratification $N > f$, which is precisely what one would expect to happen. We also see that the topography generally slopes steeper than the solid line, the semidiurnal beam, except near the shelf break, where the slopes "critically" match.

These diagonal co-phase bands correspond to what was in earlier studies identified as the "main beam." From CTD yoyo-ing at six different cross-slope positions from the shelf edge to the central Bay of Biscay, Pingree and New (1991) found strong semidiurnal signals around specific depths; connecting these large-amplitude points, they obtained a

Table 1. Estimates of characteristics slopes according to (1) for propagating internal waves at several semidiurnal and near-inertial frequencies σ and ratios N/f at mean latitudes of the BB and GMS Towed-ADCP experiments. The N/f are within the range of observed values (Fig. 7). For the semidiurnal band only discrete lunar and solar harmonics are considered. As the near-inertial band is smoothly broad, arbitrary frequencies can be chosen between [0.97, 1.06]f (van Haren, 2005).

	BB	GMS
σ, *N/f*	μ_+, μ_-	μ_+, μ_-
S_2, 27	0.0356, −0.0330	0.0676, −0.0628
S_2, 45	0.0210, −0.0201	0.0400, −0.0383
S_2, 100	0.0093, −0.0092	0.0178, −0.0174
M_2, 27	0.0328, −0.0302	0.0645, −0.0596
M_2, 45	0.0193, −0.0184	0.0381, −0.0364
M_2, 100	0.0086, −0.0084	0.0169, −0.0166
M_2, 220	0.0039, −0.0038	0.0076, −0.0076
M_4, 27	0.0915, −0.0890 (not observed)	0.1432, −0.1383 (not observed)
1.01f, 5	0.0841, −0.0096	0.1355, −0.0055
1.01f, 27	0.0067, −0.0041	0.0082, −0.0034
1.01f, 45	0.0036, −0.0027	0.0041, −0.0024
0.995f, 8	0.0219, 0.0071	0.0503, 0.0030
0.9999f, 8	0.0288, 0.0001	0.0533, 0.0001
1.00f, 8	0.0290, 0.000	0.0533, 0.000
1.00f, 27	0.0025, 0.000	0.0048, 0.000
1.00f, 45	0.0019, 0.000	0.0017, 0.000

trajectory that coincided with the theoretically predicted path of energy propagation. The very beginning of this beam, near the shelf-edge, was visualized synoptically with the towed ADCP records and supplemented by results from a linear internal-tide generation model (Gerkema *et al.,* 2004). The model, too, showed the downward-going beam clearly, and moreover demonstrated that its presence shows no seasonal dependence, as its origin lies well below the seasonal thermocline. However, this thermocline acts as a separate source of generation (in summer), because the body-force term is proportional to N^2.

If we now consider the amplitude, we see that, generally, amplitudes are large between the solid lines (Fig. 6). However, there is a "gap" near 20 km, where the amplitude drops considerably. In fact, the beam is not recognizable anymore and the amplitude shows a patchy structure, for both u and v. The individual patches show a tendency of less steep slopes, some in the direction of the dashed lines. The dashed lines are rather arbitrarily placed, but they are valid for the entire domain in all panels of Figures 5 and 6. Like the solid lines, the dashed lines correspond to sample theoretical slopes (1) for internal wave propagation, see Table 1. Their values are either: (i) for near-inertial frequencies (∼1.01f) and large-scale ($\Delta z = 100$ m) N ≈ 30f or, (ii) for semidiurnal tidal frequencies in very strong stratification of about 100f. Such strong stratification is occasionally observed when N is computed over short-scales $\Delta z = 1$ m (Fig. 7a). The latter will be clearer in GMS-data, to be described in Section 4. For the former, recall that in BB near-inertial motions are

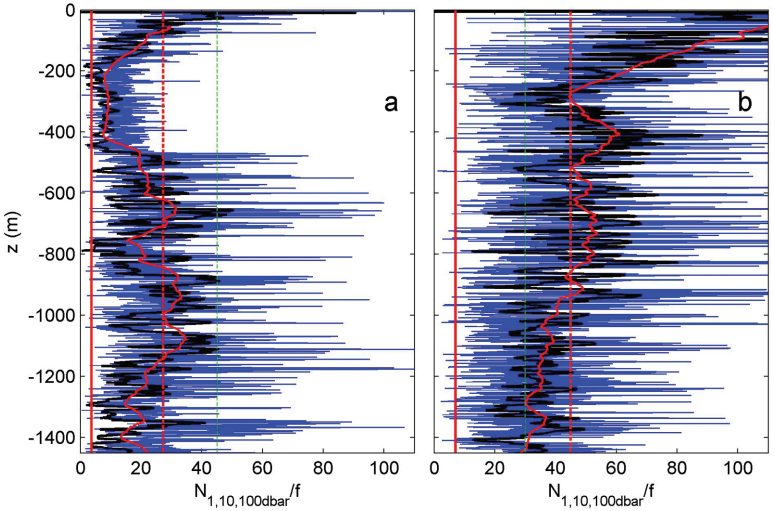

Figure 7. (a) Buoyancy frequency scaled with local inertial frequency and computed from CTD data obtained at horizontal distance 18 km in BB (end of second track, at a depth of 1720 m) over vertical scales $\Delta z = 1$(blue), $\Delta z = 10$(black) and $\Delta z = 100$(red) m. The vertical red lines indicate lower limit $N = 4f_h$ (red solid line), 27f (mean N for depth-range 500–1200 m; red-dashed) and 45f (upper-limit, mean value GMS; green-dashed lines). (b) As (a), but for GMS-data during yoyo-station at horizontal distance 12 km in towed transect, two weeks later. Here vertical lines at 27f (minimum-mean, mean value BB; green dashed) and 45f (mean for depth-range 500–1200 m; red-dashed). All N-values are excluding instabilities.

aliased into semidiurnal observations. Captions of Figures 5 and 8 give the values for σ, N combinations, taken from Table 1, Figure 7. We will only compute (1) for sample lunar and solar semidiurnal frequencies and for arbitrary frequencies from the rather broad [0.97, 1.06]f range (van Haren, 2005).

Surprisingly, there are also some spots of large amplitudes outside the main beam as well, notably near 300 m depth, between 18 and 25 km. We can only speculate about the origin of such features. The seasonal thermocline (which, as mentioned above, was identified as a separate generation region in numerical experiments) can be ruled out as a source, not only because it is weak in this time of year, but also because we see no strong signal in the thermocline (i.e. near 50 m) closer to the shelf edge, which is where it should be generated if it exists. Another idea, equally problematic, is the notion of an upward going beam originating from the shelf edge. Some theoretical models suggest the existence of such a beam, but this is because the shelf edge is in those cases modeled as a sharp corner. Numerical models adopting a smooth (realistic) slope show no such upward beam (Gerkema *et al.,* 2004); neither do observations (see Azevedo *et al.* (2006) who elaborate on this point).

So, the cause of the near-surface area of large amplitudes remains elusive. One significant element appears, however, from the phase plots, namely that the area is

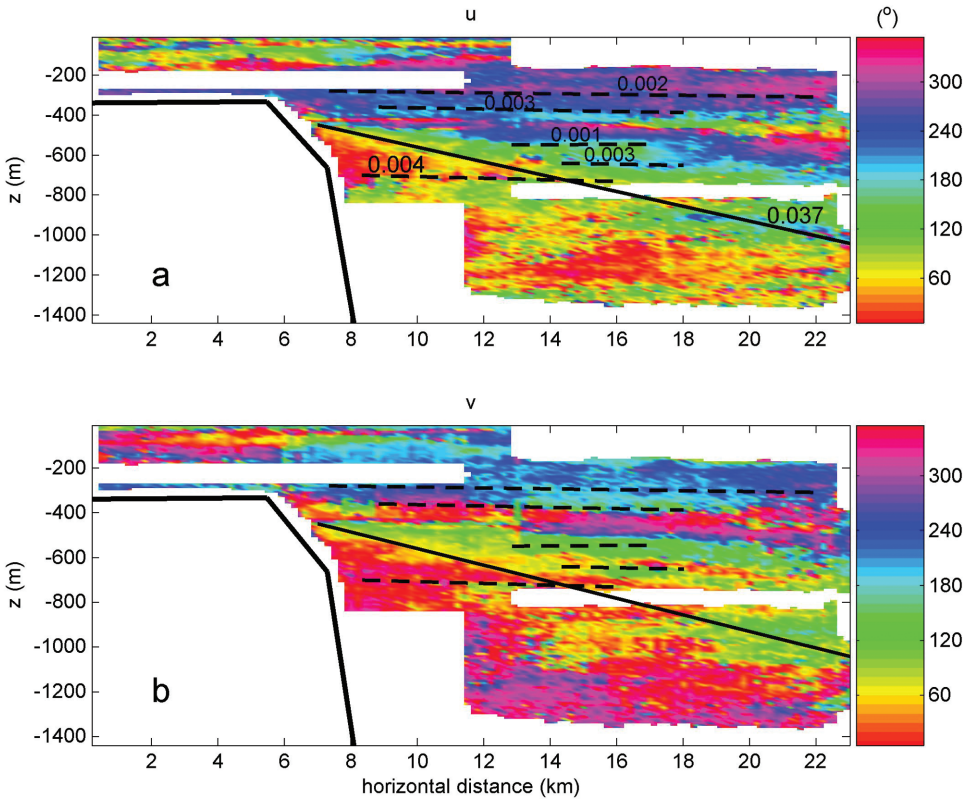

Figure 8. As Figure 5, but for GMS. Note that, as for BB, the theoretical solid and dashed curves (1), cf Table 1 and Figure 7b, are placed in rather arbitrary locations. They are valid for the entire domain and for Figures 8, 9, 10, 11 alike. The solid slope is for semidiurnal tidal motions in mean stratification or inertial motions in weak stratification (solid line, 0.037 (e.g., $\sigma = M_2$, N = 45f and σ = 1.00f, N = 10f)). Sample dashed slopes may represent near-inertial or diurnal motions in moderately strong stratification or semidiurnal motions in extremely strong, N $\approx$ 220f not observed, thin layer stratification (0.001 (e.g., σ = 1.00f, N = 60f), 0.002 (σ = 1.008f, N = 45f), 0.003 (σ = 1.01f, N = 30f and σ = 0.9999f, N = 34f) and 0.004 (σ = 1.00f, N = 30f and σ = 1.01f, N = 20f).

characterized by a uniform phase, which makes it impossible to determine in what direction it propagates, or indeed, whether it propagates at all. Between 200 and 400 m, stratification was also very low.

Finally, we notice that the phase plots for u and v (Fig. 5) are overall similar, but with a phase difference of about 90°. Moreover, the amplitude plots (Fig. 6) are similar too, except for details in the patches. This similarity suggests to a strong degree of along-slope uniformity, for if we suppose that there is no variation in this direction x, the linear momentum equation in that direction becomes du/dt = fv, implying a phase difference of 90° and an amplitude ratio equaling σ/f $\approx$ 1.31 for the semidiurnal internal tide in BB.

However, the latter is not well-observed. In Figure 5, u < v, but by about 10–15%, or half (better: square-root) of what is required from linear theory. This suggests an influence of the aliased inertial motions for which σ/f ≈ 1.0, and/or a larger alongslope variability in internal tides than expected. The latter confirms near shelf-break observations by Lam *et al.* (2004) that show considerable variability between cross-shelf transects about 10 km apart in alongslope direction.

4. Great Meteor Seamount

A towing transect was chosen above the southwestern flank of Great Meteor Seamount. Here, according to a previous study (Mohn and Beckmann, 2002), tidal motions exist with enhanced diurnal constituents (notably K_1). The direction of the two tracks perpendicular to the local slope was 213°TN (return: 33°TN), see (Fig. 2), with the starting point of the shallow track at 29°40.98′N, 28°23.38′W, where water depth is 297 m. The end of the deep (i.e. second) track lied at 29°31.74′N, 28°31.52′W, where water depth is 3365 m. During the whole measurement period of 53 hours, on 21–23 May 2006, weather and sea-state conditions were calm and favorable for towing. Spring tide was at 28 May. Unfortunately, the on-line connection with the pressure sensor failed. Due to the officer's skills we were able to sail at a near-constant speed of 3 knots, to within 0.1 knots. Despite these efforts to keep the DTV at a uniform depth, afterwards it appeared that during the sailing of the deep track the DTV had moved vertically by typically ±20 m, and sometimes even ±40 m, presumably due to deep currents off-setting the DTV. These deviations were corrected for in the analysis of the data.

Like in the Bay of Biscay, the harmonic analysis explains 70–90% of the variance (Fig. 4). The two tracks combined give a coherent picture with smooth transitions between them, both for the semidiurnal (Figs. 8, 9) and the diurnal component (Figs. 10, 11).

The semidiurnal internal tidal signal shows no clear beams, in the direction dictated by large-scale (Δz = 100 m) N, in its amplitude, and the phase lines only moderately seem to follow the direction belonging to propagation at this frequency (as indicated by the diagonal line, derived from (1)). Amplitudes u and v are of nearly the same sizes, despite the frequency ratio of σ/f ≈ 2. On the basis of Figures 8 and 9, one would be inclined to conclude that the semidiurnal internal tide is weak and incoherent along this transect, except for near-horizontal motions in the directions of dashed lines: as in BB in thin layers. Here, layering is stronger and also showing in the phase (Fig. 8), but near-inertial motions are unlikely aliased in the semidiurnal signal. So the layering would require very strong small-scale (Δz = 1–10 m) N > 100f for semidiurnal waves to propagate nearly horizontal (Table 1). Such strong small-scale stratification is only occasionally observed in CTD-data (Fig. 7b).

Yet, other measurements during the same cruise, involving combined CTD/LoweredADCP yoyoing during one day, suggest a stronger more coherent tidal signal. They were carried out at a station along this transect (at about 10 km in Figs. 8 and 9), with a view to establishing the energy fluxes of the internal tidal diurnal and semidiurnal

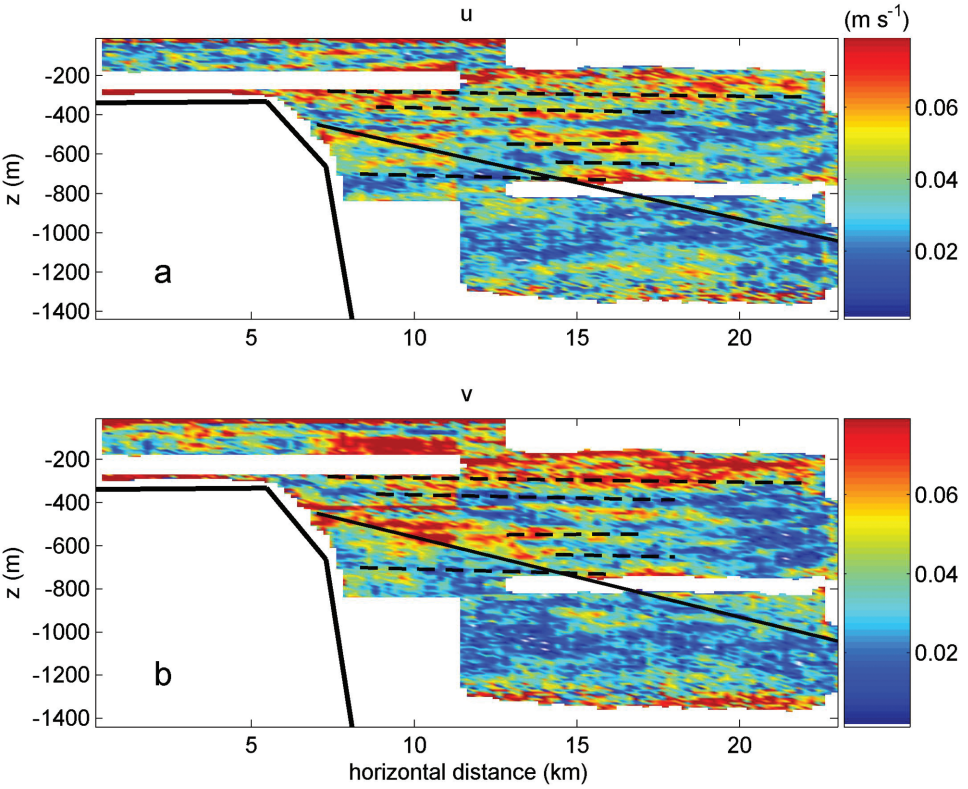

Figure 9. As Figure 6, but for GMS. Note the different color-scale compared to BB.

components (Gerkema and van Haren, 2007). At this position, the semidiurnal component was concentrated in the upper 250 m, with amplitudes up to 0.12 m s^{-1} for the cross-slope component. This seems to be in qualitative agreement with what we see near x = 10 km in Figure 8, where relatively strong currents are present between 100 and 200 m in the vertical; they are, however, not as strong as in the yoyo measurements. Part of the explanation may be that these were done at a more favorable moment in the spring-neap cycle, namely on 7 and 8 June 2006, which is halfway between the First Quarter (3 June) and Full Moon (11 June). The towed ADCP measurements, on the other hand, were carried out right after the Last Quarter (20 May).

The diurnal signal is much more pronounced (Figs. 10, 11). As noted above, here we cannot distinguish between diurnal signals of tidal origin and inertial ones, for they are very close at this latitude. In any case, this near-inertial character implies, according to (1) and Table 1, a nearly horizontal propagation of energy, coinciding with co-phase lines, and this is indeed very clearly seen in Figure 10: horizontal stripes or bands occupy the whole vertical range. The amplitude shows similar bands (Fig. 11), with the strongest signals

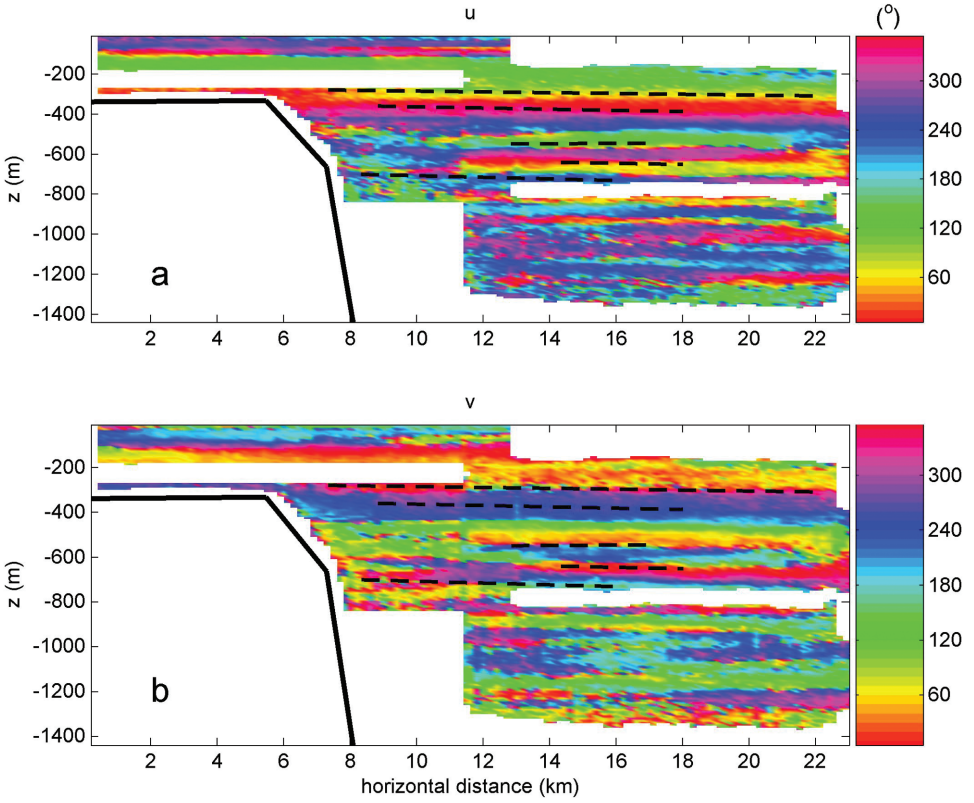

Figure 10. As Figure 8, but for diurnal motions.

being concentrated in the upper 500 m. This suggests the top of GMS acts as source. As in BB, but for the diurnal signal here, u- and v-phases differ by approximately 90°.

The signal is interspersed with thin stacked layers, notably between horizontal distances 12 and 20 km, between depths of 500 and 1000 m; these layers have thickness of the order of 10–100 m and are visible both in amplitude and in phase. They are reminiscent of the thin layers, also diurnal, found in numerical internal-tide generation experiments near critical latitudes (Gerkema *et al.,* 2006). In these experiments, they arose from a subharmonic instability of the semidiurnal internal tide; internal waves of half the frequency of M_2 (or S_2) can exist as free waves only equatorward of latitudes $\varphi = |28.8°|$ (or $|29.9°|$). Near this "critical" latitude, where the inertial frequency matches a diurnal one, semidiurnal internal tides are prone to losing energy to a diurnal subharmonic at smaller vertical scales (Hibiya *et al.,* 2002; MacKinnon and Winters, 2005). Our transect lies poleward of the critical latitude of M_2, but equatorward of that of S_2 and we cannot distinguish between these two frequencies. So, for S_2 subharmonic resonance is possible, and this would provide a cause for the weakness of the semidiurnal tide observed here, as well as for the

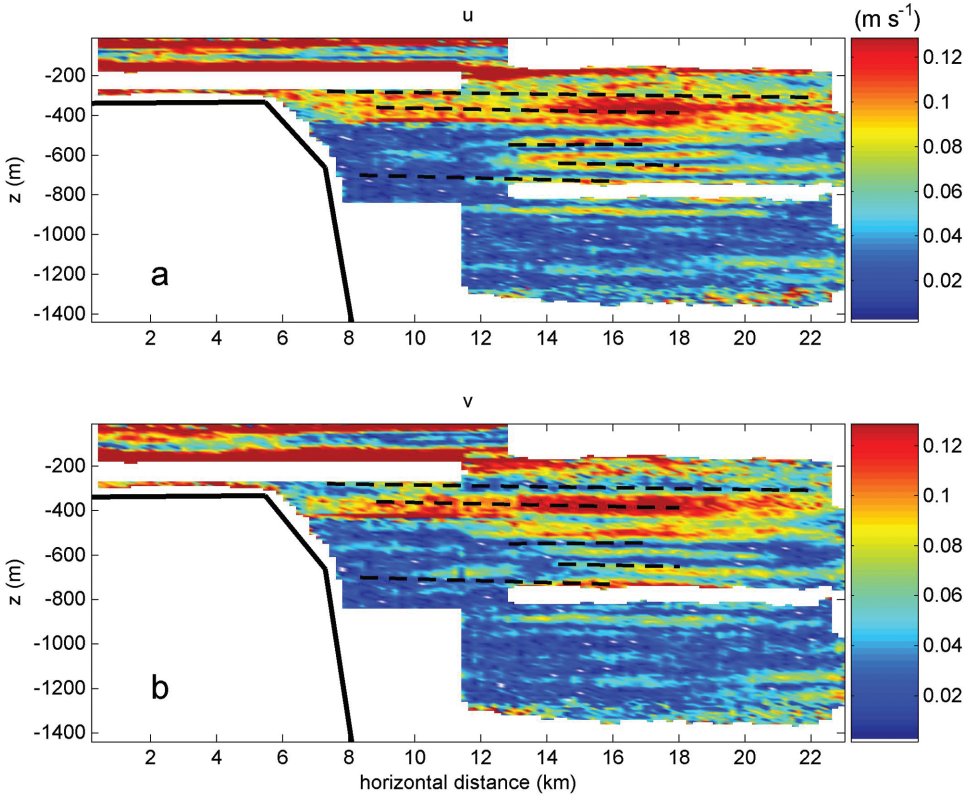

Figure 11. As Figure 9, but for diurnal motions. Note the difference color-scale compared to Figure 9.

conspicuous horizontal stripiness that we see not only in the diurnal but also in the semidiurnal signal, suggesting a dynamical connection between the two. Careful inspection shows that layers of large semidiurnal amplitude are at depths where weak diurnal/inertial amplitudes are found, and vice versa, see the zoom for cross-slope currents (Fig. 12).

This may evidence transfer of energy from large-scale semidiurnal to small-scale diurnal frequencies via sub-harmonic resonance, interpreting lack of semidiurnal energy at particular depths as directly, locally transferred to motions at half its frequency. However, it is unlikely that subharmonic resonance is the only cause for rapid alternation or patchiness in amplitude. This is because such spatial alternation was also observed between inertial and semidiurnal signals at more poleward $\varphi = 58°$N (van Haren, 2007). Also, subharmonic resonance may equally well result in a more general rather than a patchy transfer of energy to smaller scales. Furthermore, semidiurnal tidal decrease in amplitude has been observed just equatorward of the critical diurnal latitudes where near-inertial increase was observed (van Haren, 2005). Alternatively, and latitude indepen-

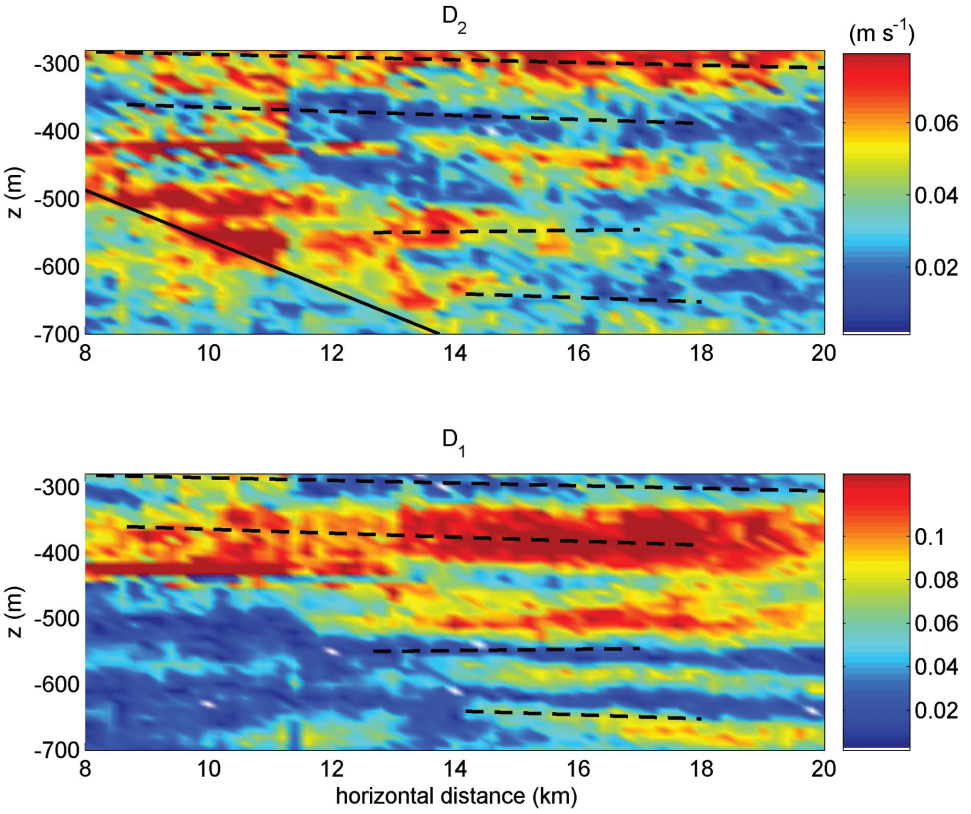

Figure 12. Zoom of Figure 9b (upper panel) and Figure 11b (lower panel): amplitudes of cross-slope motions above GMS for semidiurnal and diurnal/inertial frequencies, respectively. The straight solid (semidiurnal only) and dashed lines are identical in both panels and can be used for guidance to infer the alternating bands of enhanced/decreased amplitudes. Note the difference in color-scales.

dent, the separation in layering may be due to different trapping: super-inertial motions in near-homogeneous layers and sub-inertial motions in stratified layers (van Haren, 2006), which alternate on small scales (Fig. 7b).

5. Discussion

In summary, we have presented the results of measurements on internal waves using a towed-ADCP over a slope, at two different locations. The two locations, Great Meteor Seamount, near the latitude where the diurnal frequency matches the inertial frequency, and Bay of Biscay, where semidiurnal motions are dominant, show different and similar results, for semidiurnal motions. Different is the semidiurnal tidal beam for large-scale ($\Delta z = 100$ m) stratification and which has a limited vertical extent of several 100's of m. This beam is well observed in the Bay of Biscay including its detachment from the

continental slope, its main source. It is barely observed above Great Meteor Seamount. In the latter area, near-horizontal striped layering is more clearly observed with resolved vertical scales $\Delta z = 10–100$ m. Similar in both areas is a larger degree of patchiness observed in amplitudes more than in phases. Thus, the phase field is more coherent than the amplitude field.

We have no simultaneous local time-series to draw firm conclusions, but (as discussed in the Introduction) time-series on internal waves often show a strong intermittency, i.e. an irregular envelope modulating the wave's amplitude. From that perspective, it is not unnatural to find in a synoptic spatial view that the amplitude shows patchiness whereas the phase does not, if we can translate time into spatial variability.

Here we add the observation that the internal tide phase distribution can be more coherent than that of the corresponding amplitude field. We partly attribute rapid amplitude changes to the wave field's adiabatic response to stratification changes, N(z), see Figure 7. This phase coherence dominance also agrees with laboratory experiments performed in a non-uniformly stratified fluid that show the amplitude field of internal waves to be patchier than the corresponding phase field (Hazewinkel *et al.,* 2010). Changes in stratification changes, N(z), may affect the internal wave field in other ways as well; for instance, by genuine partial scattering, or trapping. Part of the observed horizontal distribution of the semidiurnal internal tidal amplitude fields may therefore be related to ducting of the internal wave field.

The near-horizontal layering may also be more related to the small-scale stratification. It cannot be explained from the viewpoint of intermittency, and it is also not exclusively found equatorward of critical diurnal latitudes. Nonetheless, diurnal or inertial and semidiurnal motions are observed in completely separated layering, with subsequent effects on shear and thus ocean mixing. This is best understood for inertial motions near the lower limit of the internal wave band. These motions can propagate near-horizontally in large-scale ($\Delta z = 100$ m) stratification, but their shear is concentrated in small-scale ($\Delta z = 1–10$ m) stratified layers, aligned with the wave propagation direction. In the open ocean these layers are generally persistent in time over periods longer than inertial, in certain regions up to months and extending 10's of km horizontally (e.g., Schmitt *et al.,* 1987), even when they are moved up and down by small-scale interfacial waves.

Acknowledgments. We thank the crew of the R/V *Pelagia* for the towing of the ADCP-frame. Theo Hillebrand and NIOZ-MTM prepared the instrumentation and the frame, respectively. Margriet Hiehle constructed Figure 1, Chrysanti Tsimitri took the picture in Figure 3. The bulk of the processing software has been written by IMAU (University of Utrecht) MSc students: P. van Breevoort, E. Exarchou, S. Huisman, D. Loeve, E. van Sebille and C. Tsimitri during their course of "practical oceanography."

REFERENCES

Azevedo, A., J. C. B. da Silva and A. L. New. 2006. On the generation and propagation of internal solitary waves in the southern Bay of Biscay. Deep-Sea Res. I, *53,* 927–941.

Baines, P. G. 1986. Internal tides, internal waves, and near-inertial motions, *in* Baroclinic Processes

on Continental Shelves, Coastal Estuarine Science, Vol. 3, C. N. K. Mooers, ed., AGU, Washington, DC, 19–31.

Briscoe, M. G. 1975. Preliminary results from the trimoored internal wave experiment (IWEX). J. Geophys. Res., *80,* 3872–3884.

deWitt, L. M., M. D. Levine, C. A. Paulson and W. V. Burt. 1986. Semidiurnal internal tide generation in JASIN: observations and simulation. J. Geophys. Res., *91,* 2581–2592.

Gerkema, T., F.-P. A. Lam and L. R. M. Maas. 2004. Internal tides in the Bay of Biscay: conversion rates and seasonal effects. Deep-Sea Res. II, *51,* 2995–3008.

Gerkema, T. and V. I. Shrira. 2005. Near-inertial waves in the ocean: beyond the "traditional approximation." J. Fluid Mech., *529,* 195–219.

Gerkema, T., C. Staquet and P. Bouruet-Aubertot. 2006. Decay of semi-diurnal internal-tide beams due to subharmonic resonance. Geophys. Res. Lett., *33,* L08604, doi:10.1029/2005GL025105.

Gerkema, T. and H. van Haren. 2007. Internal tides and energy fluxes over Great Meteor Seamount. Ocean Science, *3,* 441–449.

Hazewinkel J., C. Tsimitri, L. R. M. Maas and S. B. Dalziel. 2010. Observations on the robustness of internal wave attractors to perturbations. Phys. Fluids, (submitted).

Hibiya, T., M. Nagasawa and Y. Niwa. 2002. Nonlinear energy transfer within the oceanic internal wave spectrum at mid and high latitudes. J. Geophys. Res., *107,* 3207, doi:10.1029/2001JC001210.

Huthnance, J. M. and P. G. Baines. 1982. Tidal currents in the northwest African upwelling region. Deep-Sea Res. A, *29,* 285–306.

Klymak, J. M. *et al.* 2006. An estimate of tidal energy lost to turbulence at the Hawaiian Ridge. J. Phys. Oceanogr., *36,* 1148–1164.

Lam, F.-P. A., L. R. M. Maas and T. Gerkema. 2004. Spatial structure of tidal and residual currents as observed over the shelf break in the Bay of Biscay. Deep-Sea Res. I, *51,* 1075–1096.

LeBlond, P. H. and L. A. Mysak. 1978. Waves in the Ocean. Elsevier, NY, 602 pp.

Lien, R.-C. and M. C. Gregg. 2001. Observations of turbulence in a tidal beam and across a coastal ridge. J. Geophys. Res., *106,* 4575–4591.

Lueck, R. G. and T. D. Mudge. 1997. Topographically induced mixing around a shallow seamount. Science, *276,* 1831–1833.

MacKinnon, J. A. and K. B. Winters. 2005. Subtropical catastrophe: significant loss of low-mode tidal energy at 28.9°N. Geophys. Res. Lett., *32,* L15605, doi:10.1029/2005GL023376.

Magaard, L. and W. D. McKee. 1973. Semi-diurnal tidal currents at "site D." Deep-Sea Res., *20,* 997–1009.

Martin, J. P., D. L. Rudnick and R. Pinkel. 2006. Spatially broad observations of internal waves in the upper ocean at the Hawaiian Ridge. J. Phys. Oceanogr., *36,* 1085–1103.

Mohn, C. and A. Beckmann. 2002. The upper ocean circulation at Great Meteor Seamount. Part I: Structure of density and flow fields. Ocean Dyn., *52,* 179–193.

Pingree, R. D. and A. L. New. 1991. Abyssal penetration and bottom reflection of internal tidal energy into the Bay of Biscay. J. Phys. Oceanogr., *21,* 28–39.

Sandstrom, H. 1991. The origin of internal tides (a revisit), *in* Tidal Hydrodynamics, B. B. Parker, ed., JohnWiley, NY, 437–447.

Saunders, P. M. 1983. Benthic observations on the Madeira abyssal plain: currents and dispersion. J. Phys. Oceanogr., *13,* 1416–1429.

Schmitt, R. W., H. Perkins, J. D. Boyd and M. C. Stalcup. 1987. C-SALT—An investigation of the thermohaline staircase in the western tropical North-Atlantic. Deep-Sea Res. A, *34,* 1655–1665.

van Haren, H. 2004. Spatial variability of deep-ocean motions above an abyssal plain. J. Geophys. Res., *109,* C12014, doi:10.1029/2004JC002558.

—— 2005. Tidal and near-inertial peak variations around the diurnal critical latitude. Geophys. Res. Lett., *32,* L23611, doi:10.1029/2005GL024160.

—— 2006. Asymmetric vertical internal wave propagation. Geophys. Res. Lett., *33,* L06618, doi:10.1029/2005GL025499.

—— 2007. Inertial and tidal shear variability above Reykjanes Ridge. Deep-Sea. Res. I, *54,* 856–870.

van Haren, H., L. Maas and H. van Aken. 2002. On the nature of internal wave spectra near a continental slope. Geophys. Res. Lett., *29(12),* doi:10.1029/2001GL014341.

van Sebille, E., S. Huisman and D. Loeve. 2004. Students cruise report, LOCO-IW R. V. Pelagia cruise 64PE231, IMAU Utrecht, 63 pp (partially in Dutch).

Wunsch, C. 1975. Internal tides in the ocean. Rev. Geophys., *13,* 167–182.

Received: *3 September, 2008;* revised: *8 September, 2010.*